

Document downloaded from:

<http://hdl.handle.net/10251/145558>

This paper must be cited as:

Fernández-Vicente, J.; Baños Lopez, R.; Doménech Gómez, JD.; Domínguez-Horna, C.; Muñoz Muñoz, P. (04-2). Low-loss inverted taper edge coupler in silicon nitride. IET Optoelectronics. 13(2):62-66. <https://doi.org/10.1049/iet-opt.2018.5065>



The final publication is available at

<https://doi.org/10.1049/iet-opt.2018.5065>

Copyright Institution of Electrical Engineers

Additional Information

"This paper is a postprint of a paper submitted to and accepted for publication in IET Optoelectronics and is subject to Institution of Engineering and Technology Copyright. The copy of record is available at IET Digital Library"

Low-loss inverted taper edge coupler in silicon nitride

Juan Fernández^{1,2}, Rocío Baños¹, David Doménech¹, Carlos Domínguez³ and Pascual Muñoz²

¹ VLC Photonics S.L, c/ Camino de Vera s/n – 46022, Valencia – Spain – david.domenech@vlcphotonics.com

² Universitat Politècnica de València, c/ Camino de Vera s/n – 46022, Valencia – Spain – pascual.munoz@upv.es

³ Instituto de Microelectrónica de Barcelona (IMB-CNM), CSIC – Bellaterra 08193 - Spain

Abstract: An inverted lateral taper with one vertical discrete step was designed for a medium confinement silicon nitride waveguide platform in the C-band, as chip edge coupler, with predicted insertion loss of 0.58 dB. The design is supported by an extensive study to evaluate the impact of fabrication process variations in the performance of such coupler. The device was manufactured and measured, showing an insertion loss of 1.47 dB, which was traced back to fabrication process variations as cross-checked with simulations. To our knowledge, the reported edge coupler is the shortest and among the best performing found for silicon nitride platforms.

1. Introduction

Photonic integrated circuits (PICs) have great potential for communication systems, sensing, biophotonic, and optical signal processing systems, and the number of applications is growing in the recent years. In fact, they are currently employed for multiple applications such as telecom/datacom, bio- and life-sciences, avionics/aeronautics, safety, security to civil engineering and construction [1]-[6].

Despite many materials could be used to produce photonic integrated circuits (PICs), only a few have been employed to follow the path of the semiconductors electronics eco-system, with foundries, software suppliers and design house [7]. The materials used for which generic processes and offering access through multi-project wafer (MPW) runs [8] have been developed are Silicon on Insulator (SOI) [9], Indium Phosphide [10] and Silicon Nitride [11].

Although, to solve the low coupling efficiency problem to PICs, there are mainly two categories of coupling methods, the vertical coupling and the edge coupling. The vertical coupling is coupled to the waveguide through vertically incident or leaked light, and can be found in gratings [12], vertically microring [13], parabolic reflector [14], metal layers [15], and more experimental structures.

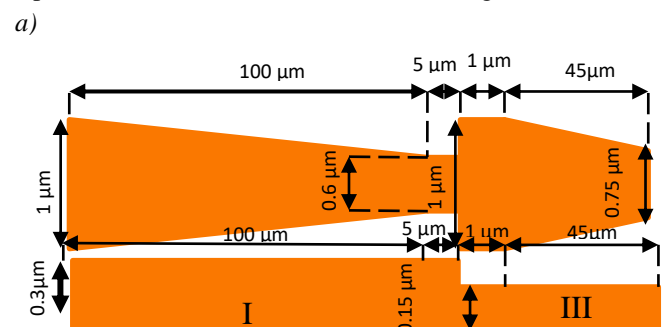
On the other hand, the edge coupling typically involves spot-size converters (SSC) [16]-[20]. Usually, inversely tapered waveguides could be used to implant an SSC. In general, inverted taper design could divide in three big groups [20]: lateral, vertical and combined (3D) inverted taper.

Silicon Nitride based integration platforms are subject of attention due to the wide wavelength range over which the material is transparent (0.4-2.4 μm) and inherently low-loss [21]. This waveguide technology is based on a combination of silicon nitride as waveguide layers, filled by and encapsulated with silica (SiO_2) as cladding layers grown on a silicon wafer. SiO_2 and Si_3N_4 layers are fabricated with CMOS-compatible industrial standard chemical vapor deposition (both low pressure, LPCVD, and plasma enhanced, PECVD) techniques, that enable cost-effective volume production [22]. Edge coupling to the chips can make use of spot-size converters (SSC) [23]-[24]. Inversely tapered waveguides, either lateral, vertical and combined (3D) [25],

waveguides are one type of SSC providing some advantages: simple design, easy fabrication, broad transmission bandwidth, and high coupling efficiency. Silicon nitride SSCs have been previously reported, with 3.3 dB insertion loss, 500 μm length and tip height 0.1 μm [26] and others with 0.65 dB losses, length of 800 μm [27] 0.150 μm tip width, and 0.7 μm tip height. Other papers quote 0.5 dB loss for film heights of 0.1 μm [28]. Moreover, there are other works based on to use UHNA3 fibers (4.1 μm core width) resulting in >90% coupling efficiency within 1.45-1.65 μm wavelength range but with waveguide thickness of 100 μm and a taper length of 500 μm [29]. In this paper, we report on the design and characterization of an inverted taper with 1.5 dB insertion loss and 150 μm length for a silicon nitride platform with guiding film height of 0.300 μm and taper tip height of 0.150 μm .

2. Device Design: Simulations and Tolerance study

The edge coupler proposed makes use of the already existing lithographic steps in our previously developed Si_3N_4 generic integration platforms [22]. That is, it does not resort to specialized additional process steps such as wet etching or more complex lithography approaches as the use of a shadow mask, but it rather markers the use of the different nitride etching levels of our platform. The mode transformer design is made up of two height levels of an adiabatic inverse lateral taper structure in silicon nitride shown in Fig.1.



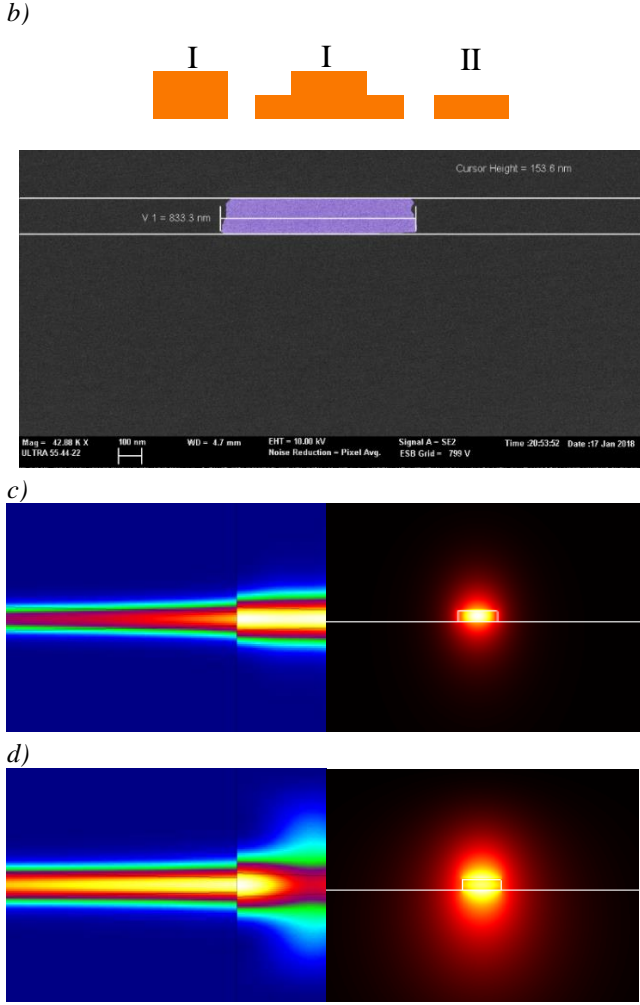


Fig. 1. (a) Top and side view of the inverted taper, (b) platform waveguide cross-sections, I deep, II shallow and III mini-deep and SEM micrograph (in pseudo-color) of the facet tip for one of the measured inverted tapers (tip widths in 0.8-0.9 μm), (c) field propagation simulation of the structure and fundamental mode of the tip for the TE polarization, (d) field propagation simulation of the structure and fundamental mode of the tip for the TM polarization.

2.1. Material and Crossection considerations

The designed device was fabricated in a Silicon Nitride photonics platform compatible with a standard CMOS pilot line. The waveguide basic structures, shown in Fig. 1, are fabricated on 100 mm silicon wafer diameter, and the layer stack is composed of a silicon oxide buffer layer (2.5 μm thick, $n=1.45$), following a LPCVD silicon nitride layer with a thickness of 0.3 μm ($n= 2.01$) acts as the core layer and finally a 2.0 μm thick silicon oxide ($n=1.45$) cladding layer. Three different waveguide structures are defined by photolithography with a I-line stepper (minimum feature 0.6 μm) followed by a reactive ion etching (RIE) of the silicon nitride film. The 0.3 μm silicon nitride layer may be etched: completely to form a strip waveguide structure (deep), partially avoiding core obtaining a rib waveguide structure (shallow) or partially in the core and completely in the sides to form a strip waveguide of 0.150 μm thickness (mini-deep).

2.2. Mode field overlap study

There are two main overlaps to study: fiber to waveguide tip overlap and edge waveguide tip to waveguide transition overlap. To obtain the insertion loss of the device, the overlap integral [30] between different widths of the three possible crosssections and a 2.5 μm Mode Field Diameter (MFD) that is typical of lensed fiber has been performed. The overlap integral $\Omega(z)$ is defined by:

$$\Omega(z) = \frac{\left| \int E_f(x, y) \int E_w(x, y, z) dx dy \right|^2}{\int |E_f(x, y)|^2 dx dy \int |E_w(x, y, z)|^2 dx dy} \quad (1)$$

Where $E_f(x, y)$ is the Gaussian approximation of lensed fiber mode and $E_w(x, y, z)$ is the waveguide mode solution.

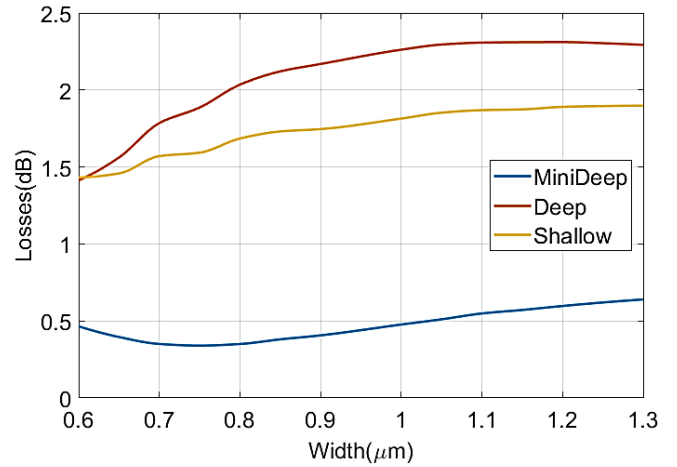
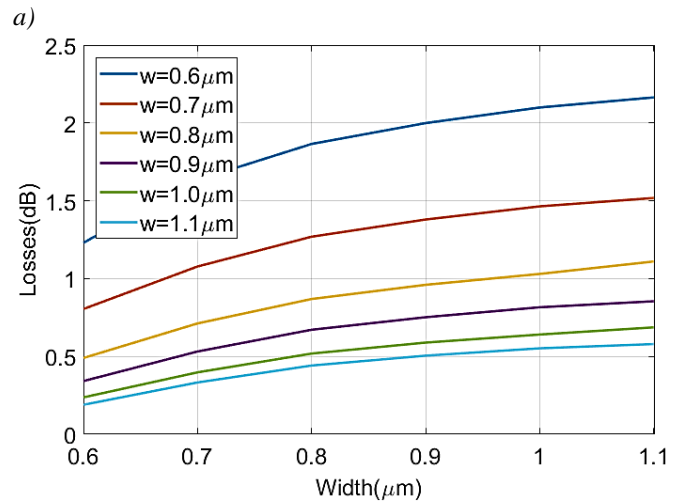


Fig. 2. Crossections response with a 2.5 μm Mode Field Diameter (MFD) in TE polarization.

Firstly, the mini-deep waveguide is the best crosssection to couple power to 2.5 μm MFD as compare with deep or shallow cross-section (see Fig. 2). There is a local minimum for the power loss of 0.35 dB with a waveguide width of 0.75 μm . Secondly, to obtain a deep cross-section output of inverted taper, an overlap integral between deep cross-section and mini-deep cross-section must be studied.



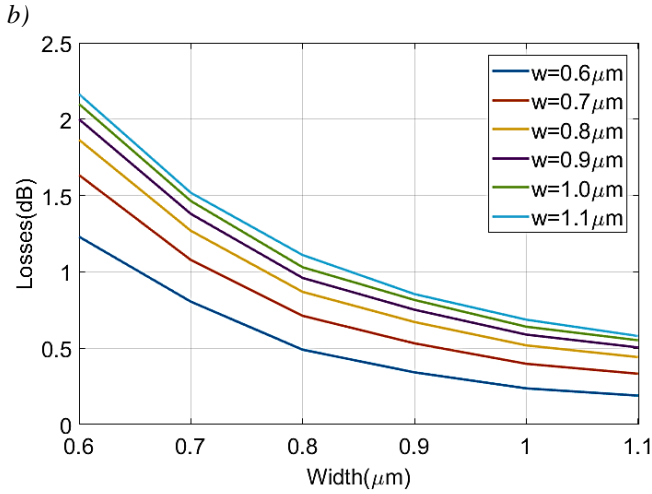


Fig. 3. *Overlap between deep waveguide and mini-deep waveguide. a) different deep widths vs mini-deep widths, b) different mini-deep widths vs deep widths.*

As shown Fig. 3 a), the loss is reduced when the deep waveguide width is increased and the mini-deep waveguide is decreased. Therefore, there is an inverse relation between these cross-section widths and the coupling loss. The mode size of the deep waveguide is larger than for the mini-deep waveguide, so the overlap loss between modes is optimized when adjusting widths as mentioned (inverse relation). Finally, from the graphs, the optimum point is for widths of 1 μm and 0.6 μm for the deep and mini-deep cross-sections respectively. These values ensure single mode operation as well.

2.3. Study of the adiabatic tapers

To optimize the excess loss of the overall device, the tapering losses must be minimized as well. The simulations in these sections are for the propagation along the complete structure in Figure 4. Firstly, the mini-deep taper starts with a 0.75 μm width, and ends with a 1 μm width, whereas the deep taper starts with a 0.6 μm width and ends with a 1 μm width. Next, the eignmode propagation method (EME) from the FIMMWAVE software package is employed to obtain the taper response and losses.

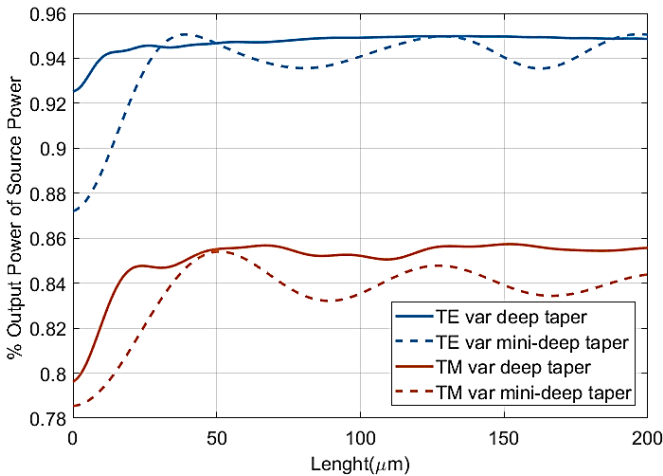


Fig. 4. *Total output power for different taper lengths for mini-deep and for deep cross-sections.*

The results are shown in Fig. 4, dashed line shows the total power coupled, for different lengths of the first taper in the mini-deep cross-section, for fixed length (100 μm) of the Deep cross-section taper. Complementary, Fig. 4 solid lines shows the results for fixed length (50 μm) of the mini-deep taper, and lengths of the Deep section taper. From the graphs, dashed line of Fig. 4 shows how the power coupling oscillates with the mini-deep taper length. At 45 μm taper length TE polarization shows a maximum. The oscillating behaviour in the power coupling vs taper length might be attributed to some mode conversion for some of the lengths as well as some mode mismatch between the two sections. That is explored and confirmed with the results shown in Fig. 5, where the 2nd order TE mode exhibits a minimum for the aforementioned 45 μm mini-deep taper length.

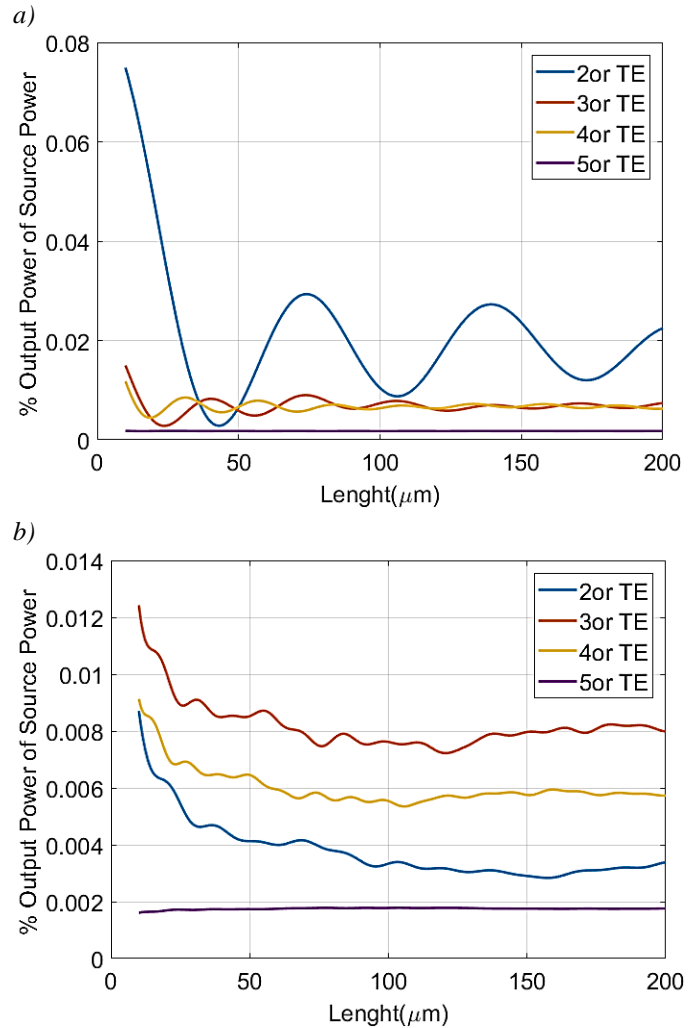


Fig. 5. *Total output power of different high order modes for different taper lengths for (a) mini-deep and (b) deep cross-sections.*

Figure 5 shows how to set the length in order to have an adiabatic taper, so higher modes are suppressed. This way, maximum power in the first order mod can be attained. In turn, Fig. 5 b) shows that the deep taper length does not significantly have impact with respect to higher order modes. For our technology, simulations show that a length above 100 μm taper length is safe. Thus, the taper lengths chosen according to all the above and to maximize coupled power are: 45 μm length for the mini-deep taper and 100 μm length

for the deep taper. With this configuration, the simulation yields 0.23 dB excess losses with a 20 dB suppression of the higher order modes.

2.4. Study of the tolerances

Optimization results into optimum design values, but nonetheless fabrication is subject to imperfection and variations. In this section, the different involved magnitudes are scanned in suitable ranges, and their impact in the coupling loss is analysed.

Defining the deep and mini-deep cross-sections in lithography makes use of two different masks that are to be aligned in different steps. To explore the impact of possible misalignments, a straight deep section is introduced in between the two tapers, as shown in Fig. 1. The misalignment can only happen in the longitudinal direction, since the mini-deep is actually done with same deep mask, but without the shallow mask protection. The extra deep length to prevent misalignments will result into extra loss, as shown in Fig. 7. Both graphs show the impact of the shallow mask shifted towards the deep section a) and mini-deep b) sections.

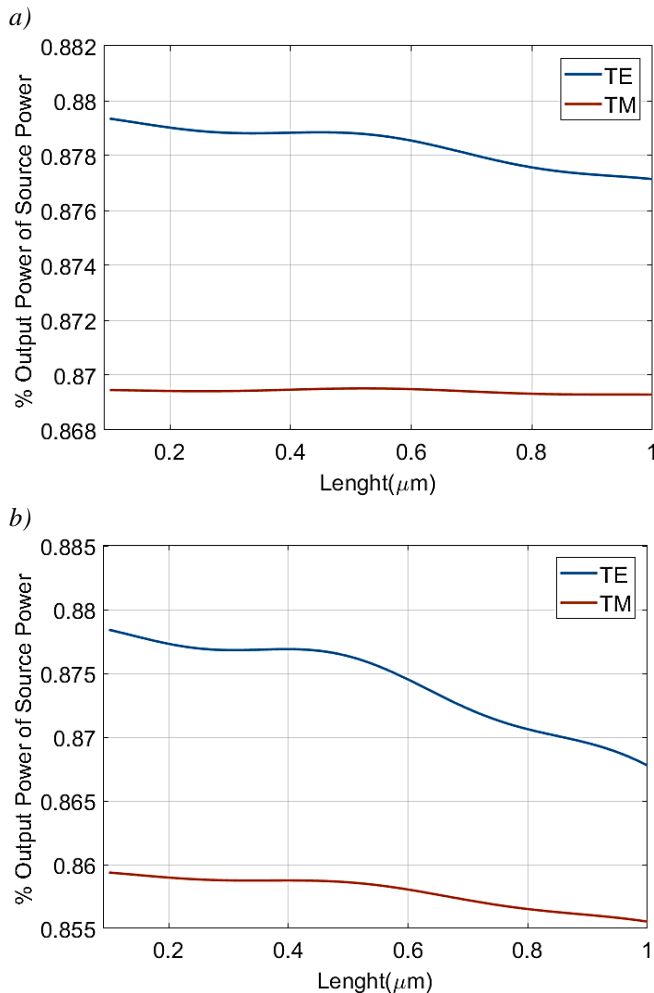


Fig. 6. (a) Shallow mask shifted towards the deep section and (b) shallow mask shifted to the mini-deep cross-section.

As shown in Figure 6 a) and b) mask alignment errors of 1 μm result into approximately 0.4 dB extra losses for the TE. The dependence of the lensed fiber MFD with the different cross-sections is analysed and shown in Fig. 7.

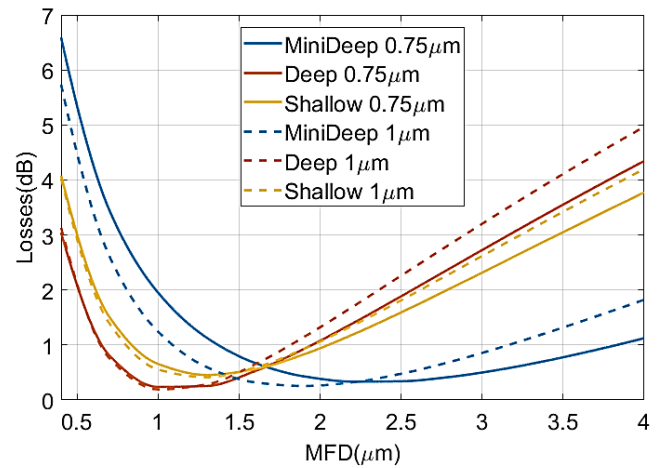


Fig. 7. MFD dependency of 0.75 μm and 1 μm width of three cross-section of TE polarization.

The mini-deep cross-section results into the lowest insertion losses for a nominal 2.5 μm MFD, as well as low loss variations for MFD changes in between 2 and 3 μm . Overall the predicted coupling loss is around 0.5 dB.

The impact of misalignment of the lensed optical fiber with respect to the taper is explored. A 1 μm offset (half of the input mode) in the two directions (X and Y direction) is taken as the maximum offset. The simulations (not shown) give little impact of the misalignment up to 1 μm , therefore we proceeded to simulate the MFD variation for a offset of 1 μm (both in X and Y). A change in MFD can be also considered as a change in Z direction (longitudinal, that is, coupling distance between the lensed fiber and the inverted taper structure).

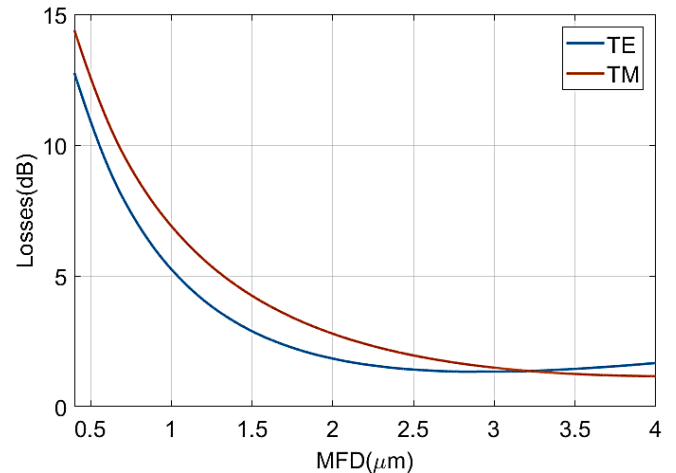


Fig. 8. Extra losses introduced for 1 μm offset for TE and TM polarization.

Figure 8 shows overlap losses due to maximum allow misalignment of 1 μm offset. In a range of incidence MFD between 2.0 and 3.0 μm , losses introduced are less than 1.812 dB. From the graph, the change in MFD (related to a change in Z, coupling distance), does not have considerable contribution to the excess loss due to the 1 μm X and Y misalignment.

The inverted taper has a broadband wavelength response, as expected from edge coupling structures. The maximum change is 0.06 dB in between 1.51 and 1.61 μm wavelength range (C and L band).

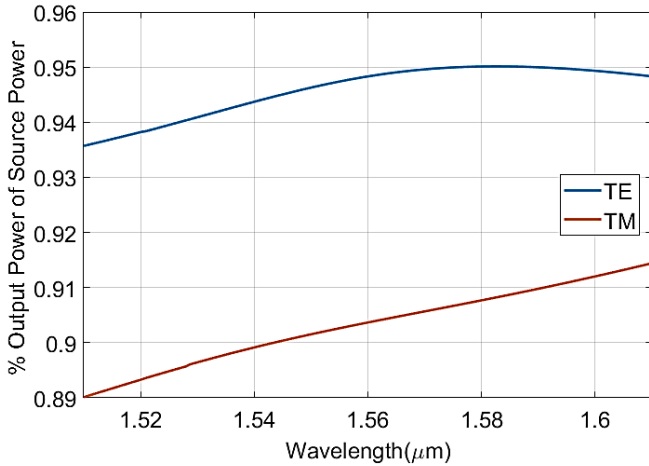


Fig. 9. Output power wavelength dependence.

This design has fabricated in the multi-project wafer run (This design was fabricated in a multi-project wafer run (MPW) offered by IMB-CNM [22] within a 5x5 mm² chip die. Instead of use DoE (Design of Experiments), only one design with optimum values is used since fabrication variations were expected, as later detailed, and with the aim of correlating experimental results to the design and simulation flow outcomes. With this structure is possible to test variations in the process also so any misalignment between masks or width errors that it will affect to response of this structure. This approach is used in order to correlate simulator, process variations and the real response of this structure. DoE will be attempted in successive manufacturing runs.

3. Experimental results

We used an end-fire measurement setup with microscope objectives with MFD 2.5 μm and with polarizers, in order to inject and collect TE polarization. The test structure is composed of two edge couplers, each at one side of the chip, and a straight deep waveguide deep of 1 μm width between them. To measure the response a ASE broadband source was employed, together with a OSA. All the measurements are normalized to the spectrum acquired without the chip, that is between the microscope objectives face to. All measurements are with the polarizers set to allow TE to go through to/from the microscope objectives. Fiber collimators are employed, so as to allow fiber connections from the ASE source and to the OSA.

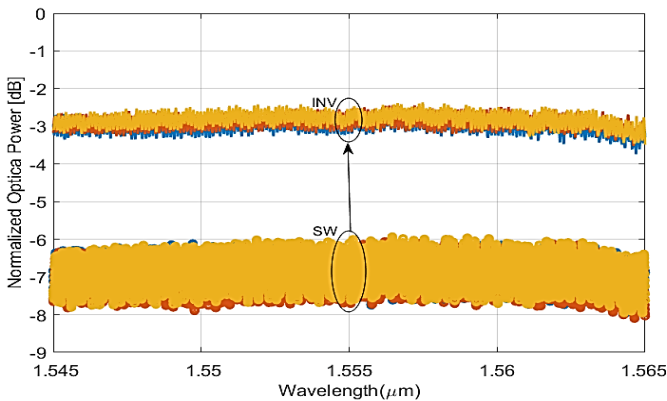


Fig. 10. Fiber to fiber TE transmission measurements for test structures with (INV) and without (SW) inverted tapers.

The results are shown in Fig. 10 both for a straight waveguide with two inverted tapers a) and without them b) as detailed. The fiber to fiber loss is 3.635 dB when inverted tapers are employed inverted taper. The measured propagation loss for the 1 μm width deep straight waveguide is 1.41 dB/cm [23] The total length between edge couplers in the chip is 4998 μm, which represent 0.7 dB of loss due to propagation. Therefore, each edge coupler has 1.47 dB insertion loss for the TE polarization. This is significantly different from the 0.58 dB predicted by simulation (0.35 dB due to overlap and 0.23 dB due to the tapers, i.e. transition loss). The difference is attributed to the following. Firstly, the wafers were stealth diced 25 μm inside the die. Therefore, the mini-deep taper was no longer 45 μm long, but its length was reduced accordingly. Simulations for the new length and result width of 0.9 μm width in the mini-deep result into additional overlap coupling loss of 0.405 dB insertion losses for TE polarization. Furthermore, the new taper length increases the taper loss up to 0.351 dB. Next, the width variations in the lithographic processes are of the order of 0.1 μm, which in turn result from simulation into an 0.295 dB in total (overlap and transition). Mask and fabrication alignment errors could add 0.4-0.5 dB as mentioned in section D1 due to misalignment between masks that produce overlap losses. To sum up, the overall losses in the worst case, including a width error, may reach 1.051 dB for TE, whereas losses due to mask alignment and fabrication may add an extra 0.4-0.5 dB. This could explain the experimental 1.47 dB vs the 0.58 dB predicted in the design stage.

4. Conclusions

A lateral inverted taper was designed for a Silicon Nitride platform, with theoretical insertion loss of 0.58 dB. Experimental results yield 1.47 dB loss, and the difference was studied incorporating into the simulation the known manufacturing variations. This structure as edge coupler is the shortest reported in silicon nitride with a length of 150 μm, and among the ones with the lowest insertion loss in the literature.

5. Acknowledgments

The authors acknowledge financial support through projects TEC2015-69787-REDT PIC4TB, TEC2016-80385-P SINXPECT, TEC2014-54449-C3-1-R, GVA PROMETEO 2017/103, EC H2020-ICT-27-2015 PICs4all CSA 68777.

6. References

- [1] Liao, Paul, ed. 'Theory of dielectric optical waveguides' 2e. Academic press, 2012.
- [2] Marcatili, Enrique AJ. 'Dielectric rectangular waveguide and directional coupler for integrated optics.' Bell System Technical Journal 48.7 (1969): 2071-2102.
- [3] Hunsperger, Robert G. 'Integrated optics', Vol. 4. Springer Verlag, 1995.
- [4] Garmire, Elsa, et al. 'Integrated optics', Vol. 7. Springer Science & Business Media, 2013.
- [5] Miller, S. E. (1969). 'Integrated optics: An introduction', Bell System Technical Journal, 48(7), 2059-2069.

- [6] Tomlinson, W. J., and C. A. Brackett. 'Telecommunications applications of integrated optics and optoelectronics.', *Proceedings of the IEEE* 75.11 (1987): 1512-1523.
- [7] Nenni, D.; McLellan, P.M. 'Fables: The Transformation of the Semiconductor Industry', CreateSpace Independent Publishing Platform: Colorado Springs, CO, USA, 2014.
- [8] Munoz, P. *et al.* 'Photonic integration in the palm of your hand: Generic technology and multi-project wafers, technical roadblocks, challenges and evolution.', In *Proceedings of the 2017 Optical Fiber Communications Conference and Exhibition (OFC)*, Los Angeles, CA, USA, 19–23 March 2017; pp. 1–3.
- [9] Lim, A.E.J.; Song, J.; Fang, Q.; 'Review of silicon photonics foundry efforts.', *IEEE J. Sel. Top. Quantum Electron.* 2014, 20, 405–416.
- [10] Smit, M.; Leijtens, X.; Ambrosius, H; *et al.* 'An introduction to InP-based generic integration technology.', *Semiconduct. Sci. Technol.* 2014, 29, 083001, doi:10.1088/0268-1242/29/8/083001.
- [11] Leinse, A.; Heideman, R.; Hoekman, M.; *et al.* 'TriPleX waveguide platform: Low-loss technology over a wide wavelength range.', In *Proceedings of Integrated Photonics: Materials, Devices, and Applications II.*; SPIE: Bellingham, WA, USA, 2013; pp. 1–13.
- [12] D. Taillaert, W. Bogaerts, P. Bienstman, 'An out-of-plane grating coupler for efficient butt-coupling between compact planar waveguides and single-mode fibers', *IEEE J. Quantum Electron.* 38, 949-955 (2002).
- [13] Wahsheh, Rami A., *et al.* "Silicon microring vertical coupler." *High-Capacity Optical Networks and Enabling Technologies (HONET)*, 2009 6th International Symposium on. IEEE, 2009.
- [14] T. Dillon, J. Murakowski, S. Shi, and D. Prather, 'Fiber-to-waveguide coupler based on the parabolic reflector', *Opt. Lett.* 33, 896-898 (2008).
- [15] H. Li, Z. Cao, H. Lu, and Q. Shen, 'Free-space coupling of a light beam into a symmetrical metal-cladding optical waveguide', *Appl. Phys. Lett.* 83, 2757 (2003).
- [16] Cardenas, Jaime, *et al.* "High coupling efficiency etched facet tapers in silicon waveguides." *IEEE Photon. Technol. Lett.* 26.23 (2014): 2380-2382.
- [17] K. Shiraiishi, H. Yoda, A. Ohshima, 'A silicon-based spot-size converter between single-mode fibers and Si-wire waveguides using cascaded tapers', *Appl. Phys. Lett.* 91, 141120 (2007).
- [18] Araghchini, M. (2008). 'Design and fabrication of efficient fiber to chip couplers', (Doctoral dissertation, Massachusetts Institute of Technology).
- [19] Tao, S. H., Song, J., Fang, Q., Yu, M. B., Lo, G. Q., & Kwong, D. L. (2008). 'Improving coupling efficiency of fiber-waveguide coupling with a double-tip coupler.', *Optics express*, 16(25), 20803-20808.
- [20] Moerman, I., Van Daele, P. P., & Demeester, P. M. (1998). 'A review on fabrication technologies for the monolithic integration of tapers with III-V semiconductor devices.', *IEEE Journal of Selected Topics in Quantum Electronics*, 3(6), 1308-1320.
- [21] P. Muñoz *et al.*, 'Silicon Nitride Photonic Integration Platforms for Visible, Near-Infrared and Mid-Infrared Applications', *Sensors*, 17(9), 2088 (2017).
- [22] Silicon nitride technology at IMB-CNM-CSIC. <http://www.imb-cnm.csic.es/index.php/en/clean-room/silicon-nitride-technology>, accessed July 2018
- [23] Papes, Martin, *et al.* "Fiber-chip edge coupler with large mode size for silicon photonic wire waveguides." *Optics express* 24.5 (2016): 5026-5038.
- [24] Cheben, Pavel, *et al.* "Broadband polarization independent nanophotonic coupler for silicon waveguides with ultra-high efficiency." *Optics express* 23.17 (2015): 22553-22563.
- [25] Moerman, I., Van Daele, P. P., & Demeester, P. M. 'A review on fabrication technologies for the monolithic integration of tapers with III-V semiconductor devices', *IEEE Journal of Selected Topics in Quantum Electronics*, 3(6), 1308-1320 (1998).
- [26] Y. Shani *et al.* 'Efficient coupling of a semiconductor laser to an optical fiber by means of a tapered waveguide on silicon', *Applied physics letters*, 55(23), 2389-2391 (1989)
- [27] M.T. Doan *et al.* 'Spot size mode converter for efficient coupling to SiN waveguides', In *Proc. Photonics North International Society for Optics and Photonics*, pp. 221-228, December 2004.
- [28] L. Zhuang *et al.* 'Low-loss, high-index-contrast Si₃N₄/SiO₂ optical waveguides for optical delay lines in microwave photonics signal processing', *Opt. Express* 19, 23162-23170 (2011)
- [29] Zhu, Tiecheng, *et al.* 'Ultrabroadband High Coupling Efficiency Fiber-to-Waveguide Coupler Using Si₃N₄/SiO₂ Waveguides on Silicon', *IEEE Photonics Journal* 8.5 (2016): 1-12.
- [30] H. Kobayashi *et al.* 'Narrow-beam divergence 1.3- μm multiple-quantum-well laser diodes with monolithically integrated tapered thickness waveguide', *IEEE Journal of Selected Topics in Quantum Electronics*, 1998, vol. 3, no 6, p. 1384-1391.